View metadata, citation and similar papers at core.ac.uk

brought to you by CORE

provided by Radboud Repository

Radboud Repository

Radboud University Nijmegen

PDF hosted at the Radboud Repository of the Radboud University Nijmegen

The following full text is a publisher's version.

For additional information about this publication click this link.
http://hdl.handle.net/2066/72303

Please be advised that this information was generated on 2017-12-06 and may be subject to change.

Role of the axial vector a_1-meson exchange in hypernuclear nonmesonic weak decays

K. Itonaga
Laboratory of Physics, Faculty of Medicine, University of Miyazaki, Kiyotake, Miyazaki 889-1692, Japan

T. Motoba
Laboratory of Physics, Osaka Electro-communication University, Neyagawa, Osaka 572-8530, Japan

T. Ueda
Arida 1891, Kita-Hiroshima, Hiroshima 731-1533, Japan

Th. A. Rijken
Institute of Mathematics, Astrophysics and Particle Physics, University of Nijmegen, The Netherlands
(Received 30 December 2007; revised manuscript received 3 March 2008; published 24 April 2008)

In the meson-theoretical potential model for the study of the nonmesonic decay rates and asymmetries of hypernuclei, for the first time, the axial-vector a_1 meson ($J^{\rm PC} = 1^{++}$, $m_{a_1} = 1230$ MeV) is introduced. The a_1 meson is the chiral partner of the ρ meson and has been treated in the meson-pair exchange framework as $\rho\pi/a_1$ and $\sigma\pi/a_1$. This is analogous to the treatment of ρ and σ exchange in our model. The a_1-meson exchange is found to give remarkable modifications of the parity-conserving decay potentials ($^{1,3}S \to {}^{1,3}S$ and ${}^3S_1 \to {}^3D_1$) at short range $r \leqslant 1$ fm. As a result, the calculated intrinsic asymmetry parameter α_Λ for ${}^5_\Lambda$He becomes very small and positive in good agreement with the recent high-quality experimental data. The calculated small values of α_Λ are well compared with the data for ${}^{11}_\Lambda$B and ${}^{12}_\Lambda$C within error bars. The inclusion of the a_1 meson also improves the Γ_n/Γ_p ratios and leads to a consistent explanation for the existing nonmesonic weak decay data of the light Λ hypernuclei ($A \leqslant 12$). The results calculated in the $\pi + 2\pi/\rho + 2\pi/\sigma + \omega + K + \rho\pi/a_1 + \sigma\pi/a_1$ exchange interaction model are presented together with the estimates without a_1. Also, the derivation of the expression for the proton asymmetry is described in some detail to elucidate the calculation procedures and phase conventions.

DOI: 10.1103/PhysRevC.77.044605 PACS number(s): 13.75.Ev, 13.30.Eg, 21.80.+a, 21.30.−x

I. INTRODUCTION

The hypernuclear nonmesonic weak decay provides a unique opportunity for understanding the hyperon-nucleon weak interaction $\Lambda N \to NN$ with the strangeness change $\Delta S = 1$. High-quality data obtained with advanced techniques have been reported in recent years from KEK and they are challenges for the theoretical understanding of the weak interaction mechanisms. The recent improved data of the ratio of the neutron-stimulated decay rate $\Gamma_n(\Lambda n \to nn)$ to the proton-stimulated one $\Gamma_p(\Lambda p \to np)$ (n/p ratio) tend to converge to $\simeq$0.5 for ${}^5_\Lambda$He and ${}^{12}_\Lambda$C [1–3]. The data of the asymmetry parameter of the proton emitted in the nonmesonic decay from the polarized hypernuclear states are found to be very small for ${}^5_\Lambda$He and for the mixture of ${}^{12}_\Lambda$C and ${}^{11}_\Lambda$B [1,4–6]. In light of such high-quality and high-statistics data on a variety of observables, it is to be expected that theoretical models need to cover new types of exchanges in terms of the mesonic quantum numbers $J^{\rm PC}$.

In the last decade many theoretical studies on the weak $\Lambda N \to NN$ interaction have been devoted to understand the decay observables such as the total decay rate $\Gamma_{nm} = \Gamma_p + \Gamma_n$, the n/p ratio, and the decay proton asymmetry on the basis of the meson-exchange models. Among others, the correlated-2π exchange mechanism was first proposed in Ref. [7], and various refinements have been carried out [8,9]. The meson-exchange models have been further extended by several authors [10–13], while new attempts have been made in the direct-quark model [14,15] and the effective-field theory [16,17].

Among the nonmesonic decay observables, for a long time it was puzzling to explain the large experimental n/p ratio and the very small proton asymmetry parameter. However, at present there seems to be a consensus that the π- and K-meson exchange interactions play an important role in explaining the large n/p ratio.

On the other hand, nowadays the unraveling of the problem of the decay asymmetry is controversial. It has been difficult to understand both the sign and magnitude of the proton asymmetry parameter in spite of many theoretical attempts such as meson-exchange models and direct-quark model [9,10,12,15,18–20]. Parreño *et al.* [16] applied the effective field theory in which they introduced the contact interactions with phenomenological parameters together with the π- and K-exchange interactions and attempted to determine the coupling parameters by fitting the experimental data. They pointed out [16] that the scalar-isoscalar interaction of the contact term is important to fit the asymmetry parameters well. Then Sasaki *et al.* [21] include the σ-meson exchange in their model of meson exchange plus quark-quark interaction and treat the $\Lambda N\sigma$ weak and $NN\sigma$ strong vertices phenomenologically with adjustable coupling constants so as to understand the asymmetry parameter of ${}^5_\Lambda$He. Recently Chumillas *et al.* [22] show that the uncorrelated and correlated 2π exchange interactions may play a role in understanding the asymmetry parameter. All these articles stress that the scalar-isoscalar

 ©2008 The American Physical Society

type of interactions, such as σ exchange, the exchange of the correlated 2π coupled to σ, and uncorrelated 2π exchanges, are especially important in explaining the asymmetry.

Barbero *et al.* [23] adopted as a model pseudoscalar and vector-meson exchanges plus the σ-meson exchange, and treated the weak and strong coupling constants of the σ meson as adjustable parameters in the same manner as in Ref. [21]. However, they could not explain the data of asymmetry and other observables of ${}^{5}_{\Lambda}$He simultaneously.

In Refs. [7–9], we have shown that $2\pi/\sigma$ and $2\pi/\rho$ exchanges are important in understanding the decay rates and the n/p ratios of light Λ hypernuclei, although the $2\pi/\sigma$ exchange interaction does not play a favorable role in explaining the asymmetry parameter of ${}^{5}_{\Lambda}$He [9]. Our $\pi + 2\pi/\rho + 2\pi/\sigma + \omega + K$ exchange model gives large negative values in contrast to the very small asymmetry parameters observed for ${}^{5}_{\Lambda}$He and ${}^{12}_{\Lambda}$C. In addition to this discrepancy, this model gives large n/p ratios that overshoot the experimental data for those light Λ hypernuclei. These results clearly indicate that new ingredients are needed to improve our model. In the above model, the central forces in the ${}^1S_0 \to {}^1S_0$ and ${}^3S_1 \to {}^3S_1$ channels are too strong with a positive sign, whereas the tensor force in the ${}^3S_1 \to {}^3D_1$ channel is rather strong with a negative sign. The strong central force nature originates dominantly from the $2\pi/\sigma$ exchange interaction, whereas the strong tensor force is due to the total effect of the π, K, and $2\pi/\rho$ exchange interactions.

To try to solve the discrepancy between theory and experiments for the asymmetry, we extend the meson theoretical approach of Refs. [7–9] by taking new types of the exchanged mesonic quantum numbers into account. As an important step in this program we introduce, in this article for the first time, the axial-vector a_1-meson exchange in addition to the previous model of $\pi + 2\pi/\rho + 2\pi/\sigma + \omega + K$ exchanges. The a_1 meson has spin-isospin $J^{\rm PC} = 1^{++}, T = 1$ and is a chiral partner of the vector ρ meson ($J^{\rm PC} = 1^{--}, T = 1$), as the scalar σ meson ($J^{\rm PC} = 0^{++}, T = 0$) is a chiral partner of the pseudoscalar π meson ($J^{\rm PC} = 0^{-+}, T = 1$). Here we study the nonmesonic weak decay in this extended meson-exchange model. We note that the model of Refs. [7–9] is a kind of one-boson-exchange (OBE) model with form factors. The weak $\Delta S = 1$ vertices of the heavy mesons are generated via their (strong) decays and the weak pion coupling.

Recently one of the authors (Th.A.R.) and Yamamoto presented the new version of the baryon-baryon interaction model ESC04 of the strangeness $S = 0, -1$, and -2 sectors [24,25]. The nucleon-nucleon and hyperon-nucleon interactions of ESC04 model contain axial-vector meson and meson-pair exchanges, which improve the fit of NN-scattering data substantially, having a very small $\chi^2/N_{\rm data}$. The axial-vector a_1-meson exchange and the meson-pair $(\pi\rho)_1$ exchange are found to produce spin-spin and tensor forces with sizable contributions at short range.

The success of the ESC04 model inspired us to take into account the axial-vector a_1-meson exchange also in our model. We incorporate the a_1-meson exchange in the $\Lambda N \to NN$ via the strong coupling of a_1 to ρ and π in the intermediate state, which we denote as $\rho\pi/a_1$ exchange. Similarly there is the contribution via the strong coupling of a_1 to σ and π ($\sigma\pi/a_1$ exchange). This treatment of a_1 exchange is akin to that of ρ and σ exchange. The $\rho\pi/a_1$ and the $\sigma\pi/a_1$ exchange potentials modify the short-range behavior of the total decay potential dramatically and thus the new total decay potential appears very successful in understanding the data of the asymmetry and the n/p ratios of light Λ hypernuclei simultaneously.

The article is organized as follows. In Sec. II, we present the angular distribution of a proton emitted in the nonmesonic decay from the polarized hypernuclei and define the asymmetry parameter of a proton in the framework of shell model, where the transition amplitudes starting from the ΛN-relative s state are given explicitly on the basis of the adopted phase conventions. In Sec. III, the extended meson-exchange model is presented in detail. The axial-vector a_1-meson exchanges are introduced in terms of $\rho\pi/a_1$ and $\sigma\pi/a_1$ exchanges. The coupling Hamiltonians are given and the adopted coupling constants and parameters are explained and shown. In Sec. IV, first the features of the a_1-meson exchange interaction are discussed to elucidate its effects on the decay observables. Then, the numerical evaluations of the decay rates, the n/p ratios, and the decay asymmetry parameters are presented and compared with the ${}^{5}_{\Lambda}$He, ${}^{11}_{\Lambda}$B, and ${}^{12}_{\Lambda}$C hypernuclear decay data. Finally, a summary and outlook are given in Sec. V.

II. ANGULAR DISTRIBUTION OF A PROTON AND ASYMMETRY PARAMETER

When the hypernucleus is produced in the (π^+, K^+), (K^-, π^-), and (γ, K^+) reactions, the produced excited states and/or the ground state are generally polarized. Excited states below the particle emission threshold de-excite through the γ transitions and cascade down to the ground state. Thus the hypernuclear ground state is populated and acquires the certain amount of polarization P_H [26,27]. Then the hypernucleus undergoes weak decay such as either mesonic or the nonmesonic decay. In this article we confine ourselves to the nonmesonic weak decays from the polarized hypernuclear ground state.

The vector polarized hypernuclear state is expressed in the density matrix as

$$\rho = \frac{1}{2J_H + 1}\left[1 + \frac{3}{J_H + 1}(\boldsymbol{P}_H \cdot \boldsymbol{J}_H)\right], \tag{1}$$

where J_H is a hypernuclear spin and $\boldsymbol{P}_H$ is a hypernuclear polarization that is directed to the unit vector $\hat{\boldsymbol{n}}$ which is normal to the reaction plane, that is, $\boldsymbol{P}_H = P_H\hat{\boldsymbol{n}}$.

The angular distribution of the proton emitted in the nonmesonic decay of the polarized hypernucleus is evaluated by taking the trace of the density matrix of Eq. (1), with fixing the angles of the outgoing proton momentum $\hat{\boldsymbol{k}}_p$ as

$$\frac{d\Gamma(J_H, T_H, P_H \to \hat{\boldsymbol{k}}_p, \nu_p)}{d\Omega_{\boldsymbol{k}_p}} = \frac{2\pi}{\hbar}\,{\rm tr}\,(M\rho M^\dagger). \tag{2}$$

Here M is the nonmesonic weak decay transition matrix connecting the initial hypernuclear state and the final residual nucleus plus outgoing neutron and proton state. Inserting

Eq. (1) into Eq. (2), we obtain

$$\frac{d\Gamma(J_H, T_H, P_H \to \hat{\boldsymbol{k}}_p, \nu_p)}{d\Omega_{\hat{\boldsymbol{k}}_p}} = \Gamma_0 + P_H \Gamma_1 \cos\theta_{k_p} = \Gamma_0\big(1 + P_H \alpha_1 \cos\theta_{k_p}\big) \quad (3)$$

and

$$\alpha_1 = \frac{\Gamma_1}{\Gamma_0} \quad (4)$$

is the asymmetry parameter of a proton in the nonmesonic decay [18,20]. θ_{k_p} is the angle between the direction of emitted proton momentum $\boldsymbol{k}_p$ and the polarization direction $\hat{\boldsymbol{n}}$. Γ_0 is equivalent to $\Gamma_p/4\pi$ and Γ_p is the proton-stimulated nonmesonic decay rate from the unpolarized hypernuclear state. Γ_1 is given below. Hereafter we adopt the notation $\boldsymbol{k}_p = \boldsymbol{k}_2$ and use convention that the outgoing neutron and proton have the momentum $\boldsymbol{k}_1$ and $\boldsymbol{k}_2$, respectively, corresponding to the elementary process of $\Lambda + p \to n + p$.

$$\Gamma_1 = \frac{2\pi}{2J_H+1}\frac{3}{J_H+1}\sum_{J_1'M_1'\alpha_1'}\sum_{T_1'M_{T_1'}}\sum_{S_2'M_{S_2'}}\sum_{M_H}\int\frac{d\boldsymbol{k}_1}{(2\pi)^3} \times \int\frac{k_2^2 dk_2}{(2\pi)^3}\delta(E_f - E_i)\left|\left\langle\sum_{T_2'M_{T_2'}} {}^{A-2}\Phi_{J_1'M_1'\alpha_1',T_1'}\frac{1}{\sqrt{2}}\right.\right. \times\big[1-(-1)^{S_2'+T_2'}P_x\big]e^{i\boldsymbol{k}_1\cdot\boldsymbol{r}_1}e^{i\boldsymbol{k}_2\cdot\boldsymbol{r}_2}\chi^{S_2'}_{M_{S_2'}}\xi^{T_2'}_{M_{T_2'}} \times\left|\sum_{i,k}V_{nm}(i,k)\left|{}^{A}_{\Lambda}\Psi; J_H M_H, T_H M_{T_H}\right\rangle\right|^2 \times M_H. \quad (5)$$

The energy conservation δ function is expressed as

$$\delta(E_f - E_i) = \delta\left(\frac{\boldsymbol{k}_1^2}{2M_N} + \frac{\boldsymbol{k}_2^2}{2M_N} + E_x(A-2, J_1'T_1'\alpha_1') + \frac{(\boldsymbol{k}_1+\boldsymbol{k}_2)^2}{2M_{A-2}} + M_N - M_\Lambda - \varepsilon_N - \varepsilon_\Lambda\right), \quad (6)$$

in which the recoil energy of the residual nucleus is taken into account and the residual nuclear mass $M_{A-2} = (A-2)M_N$ is used for simplicity. The $E_x(A-2, J_1'T_1'\alpha_1')$ means the excitation energy of the residual nucleus and ε_N and ε_Λ are minus separation energy of a nucleon and a Λ hyperon in the hypernucleus, respectively. It is assumed that the hypernuclear state $|{}^{A}_{\Lambda}\Psi; J_H M_H, T_H M_{T_H}\rangle$ is written in the weak coupling model as

$$\left|{}^{A}_{\Lambda}\Psi; J_H M_H, T_H M_{T_H}\right\rangle = \left|\left[{}^{A-1}\Phi_{J_c T_c \alpha_c}\cdot\phi_{j_\Lambda t_\Lambda}\right]; \times J_H M_H, T_H M_{T_H}\right\rangle \quad (7)$$

and the nuclear core part is described in the harmonic oscillator (HO) shell model. The Λ hyperon state $\phi_{j_\Lambda t_\Lambda}$ is obtained as the solution of the cluster model or the DDHF equation of the core-nucleus $+\Lambda$ system, which is the same as that used in Ref. [8].

Γ_1 of Eq. (5) is evaluated in the proton-helicity frame where the quantization axis z is taken to be parallel to the outgoing proton momentum $\boldsymbol{k}_2$ [18,20]. The relative and center-of-mass radial vectors and the momentum vectors for the two-baryons are defined, respectively, as

$$\boldsymbol{r} = \boldsymbol{r}_1 - \boldsymbol{r}_2, \quad \boldsymbol{R} = \frac{\boldsymbol{r}_1 + \boldsymbol{r}_2}{2} \quad (8)$$

and

$$\boldsymbol{k} = \frac{\boldsymbol{k}_1 - \boldsymbol{k}_2}{2}, \quad \boldsymbol{K} = \boldsymbol{k}_1 + \boldsymbol{k}_2. \quad (9)$$

By taking into account the energy conservation [see Eq. (6)] and by fixing the direction of the outgoing proton momentum $\boldsymbol{k}_2$, we adopt three independent integral variables [20] as

$$k_2, \quad \theta_{k_1}, \quad \phi_{k_1}. \quad (10)$$

The Γ_1 of Eq. (5) is rewritten as

$$\Gamma_1 = \frac{2\pi}{2J_H+1}\frac{3}{J_H+1}\sum_{J_1'M_1'\alpha_1'}\sum_{T_1'M_{T_1'}}\sum_{S_2'M_{S_2'}}\sum_{M_H}\frac{1}{(2\pi)^6} \times\int d\big(\cos\theta_{k_1}\big)d\phi_{k_1}\int_0^{k_2^{\max}}dk_2 \times\frac{(A-2)M_N k_1^2 k_2^2}{\sqrt{(A-1)(A-2)k_Q^2 - k_2^2[(A-1)^2 - \cos^2\theta_{k_1}]}} \times\left|\left\langle\sum_{T_2'M_{T_2'}} {}^{A-2}\Phi_{J_1'M_1'\alpha_1',T_1'}\frac{1}{\sqrt{2}}\big[1-(-1)^{S_2'+T_2'}P_x\big]\right.\right. \times e^{i\boldsymbol{k}\cdot\boldsymbol{r}}e^{i\boldsymbol{K}\cdot\boldsymbol{R}}\chi^{S_2'}_{M_{S_2'}}\xi^{T_2'}_{M_{T_2'}}\left|\sum_{i,k}V_{nm}(i,k)\right| \times{}^{A}_{\Lambda}\Psi; J_H M_H, T_H M_{T_H}\left.\right\rangle\right|^2 \times M_H. \quad (11)$$

Here, the following relations are used.

$$k_Q = \sqrt{2M_N\big[M_\Lambda - M_N + \varepsilon_N + \varepsilon_\Lambda - E_x(A-2, J_1'T_1'\alpha_1')\big]}, \quad (12)$$

$$k_1 = \frac{-k_2\cos\theta_{k_1} + \sqrt{(A-1)(A-2)k_Q^2 - k_2^2[(A-1)^2 - \cos^2\theta_{k_1}]}}{A-1}, \quad (13)$$

$$k_2^{\max} = \sqrt{\frac{A-2}{A-1}}k_Q, \quad (14)$$

$$4k^2 = k_1^2 + k_2^2 - 2k_1k_2\cos\theta_{k_1}, \quad (15)$$

$$K^2 = k_1^2 + k_2^2 + 2k_1k_2\cos\theta_{k_1}, \tag{16}$$

$$\phi_k = \phi_K, \tag{17}$$

$$\cos\theta_k = \frac{1}{2k}(-k_2 + k_1\cos\theta_{k_1}), \tag{18}$$

$$\cos\theta_K = \frac{1}{K}(k_2 + k_1\cos\theta_{k_1}). \tag{19}$$

The Γ_1 is expressed in terms of the two-body transition amplitudes and in the case of ΛN relative s wave in the shell-model framework, which is given in the Appendix.

For the shell-model configurations of ${}^{5}_{\Lambda}$He ($A = 5$, $J_H = 1/2^+$) and ${}^{12}_{\Lambda}$C ($A = 12$, $J_H = 1^-$), further manipulation of Γ_1 of Eq. (A1) in the Appendix leads to the expression, as follows, in terms of Block-Dalitz notations of the transition amplitudes (a, b, c, d, e, and f) [28] as

$$\begin{aligned}\Gamma_1 = {} & \frac{4M_N}{2J_H+1}\frac{3}{J_H+1}\times 2\sum_{n_a\ell_a j_a}\frac{1}{4\pi}\int d(\cos\theta_{k_1})d\phi_{k_1}\int_0^{k_2^{\max}} dk_2 \\ & \times \frac{(A-2)k_1^2k_2^2}{\sqrt{(A-1)(A-2)k_Q^2(j_a) - k_2^2\left[(A-1)^2 - \cos^2\theta_{k_1}\right]}} \\ & \times \sum_{nN}\sum_{n'N'}\sum_{n_\Lambda n'_\Lambda}(-1)^{L-\lambda}M_{\lambda=\ell_a=L}(n_a\ell_a n_\Lambda 0; n0NL; \\ & \times M_N, M_\Lambda)c(n_\Lambda)(-1)^{L-\lambda}M_{\lambda=\ell_a=L}(n_a\ell_a n'_\Lambda 0; n'0N'L; \\ & \times M_N, M_\Lambda)c(n'_\Lambda)(-1)^{N+N'}(-i)^{L-L}\phi_{NL=\ell_a}\left(K, \frac{1}{b_R}\right) \\ & \times \phi_{N'L=\ell_a}\left(K, \frac{1}{b_R}\right)A(n_a\ell_a j_a)\frac{2\sqrt{3}}{4\pi}Re\{[ae^* - b \\ & \times (c - \sqrt{2}d)^*/\sqrt{3} - f(\sqrt{2}c + d)^*]\cos\theta_k\}\end{aligned} \tag{20}$$

and the coefficient $A(n_a\ell_a j_a)$ is given as

$${}^{5}_{\Lambda}\text{He} : A = 1/2, \quad \text{for} \quad n_a\ell_a j_a = 0s_{1/2} \tag{21}$$

$$\begin{aligned}{}^{12}_{\Lambda}\text{C} : A &= -1/2, \quad \text{for} \quad n_a\ell_a j_a = 0s_{1/2} \\ &= -1, \quad \text{for} \quad n_a\ell_a j_a = 0p_{3/2}.\end{aligned} \tag{22}$$

In deriving the expression of Eq. (20), we assume that the core-part nuclear wave functions are described in the lowest HO shell-model configurations. The $k_Q(j_a)$ corresponds to the value of k_Q in Eq. (12) in case that the average excitation energy is used in place of $E_x(A-2, J'_1T'_1\alpha'_1)$ when the excited state with $(J'_1T'_1\alpha'_1)$ is reached by picking up the nucleon in the $(n_a\ell_a j_a)$ orbit from the $(A-1)$-core nucleus. The notations a, b, c, d, e, and f signify the transition amplitudes of the six channels [28] defined for

$$\begin{aligned}&\left\langle i^{\ell_0} j_{\ell_0}(k,r)\mathcal{Y}_{\ell_0 S'_2\mathcal{J}}\xi^{T'_2}_{\nu_p+1/2}\right| V_{nm}(\Lambda N - NN) \\ &\left|\phi_{n\ell=0}(r,b_r)\mathcal{Y}_{\ell=0S\mathcal{J}=S}\xi^{T_2=1/2}_{\nu_p}\right\rangle.\end{aligned} \tag{23}$$

The α_1 defined in Eq. (4) is the asymmetry parameter of a proton with respect to the hypernuclear-spin polarized state with P_H. It is, however, often that the intrinsic asymmetry parameter α_Λ of a proton with respect to the Λ-hyperon-spin polarized state with P_Λ is defined through the relation,

$$\mathcal{A} = P_H\alpha_1 = P_\Lambda\alpha_\Lambda. \tag{24}$$

The P_H and P_Λ are related with each other [26,27]. If one assumes the weak-coupling structure for the hypernuclear state of Eq. (7) in which a Λ hyperon is in the $j_\Lambda = s^\Lambda_{1/2}$ state, the following relation applies [26,29]

$$\begin{aligned}P_\Lambda &= -\frac{J_H}{J_H+1}P_H, \quad \text{if} \quad J_H = J_c - 1/2 \\ &= P_H, \quad \text{if} \quad J_H = J_c + 1/2.\end{aligned} \tag{25}$$

Then it follows from Eq. (24)

$$\begin{aligned}\alpha_\Lambda &= -\frac{J_H+1}{J_H}\alpha_1, \quad \text{if} \quad J_H = J_c - 1/2 \\ &= \alpha_1, \quad \text{if} \quad J_H = J_c + 1/2.\end{aligned} \tag{26}$$

The intrinsic asymmetry parameter α_Λ gives a more intuitive interpretation for the asymmetry, because the asymmetry originates dominantly from the elementary weak interaction between a Λ hyperon and a proton inside the hypernucleus.

III. DESCRIPTION OF A_1-MESON EXCHANGE WEAK INTERACTION

The motivation of introducing the axial-vector a_1 meson into the $\Lambda N \to NN$ weak interaction is described in the second half of the Introduction. The a_1 meson has $J^{\text{PC}} = 1^{++}$ and the mass is 1230.0 MeV. The a_1 meson is a chiral partner of the ρ meson just like the σ meson is a chiral partner of the π meson. Therefore, it is natural to consider the chiral meson pair properly in the meson theoretical weak baryon-baryon interaction. Because for a_1 exchange we include only diagrams with the $\rho\pi$ and $\sigma\pi$ decay interactions, the range is comparable with that of, e.g., ω exchange. The potential behavior at short range is very influential in the nonmesonic weak decays due to the high momentum transfer involved. It is especially noted that the proton asymmetry originates from the interferences between the parity-conserving and the parity-violating amplitudes and, therefore, signs and magnitudes of the decay interaction potentials are crucial for the asymmetry parameter.

We treat the a_1-meson exchange through the $\rho\pi/a_1$ exchange and $\sigma\pi/a_1$ exchange processes between Λ and the nucleon. Two types of the exchange diagrams are considered for $\rho\pi/a_1(A)$ and $\rho\pi/a_1(B)$ exchanges as shown in Figs. 1(a) and 1(b), respectively. In Fig. 1(a), a nucleon is considered in the intermediate baryon state, while in Fig. 1(b) a Σ baryon is considered. The $\sigma\pi/a_1$ exchange diagram is depicted in Fig. 2.

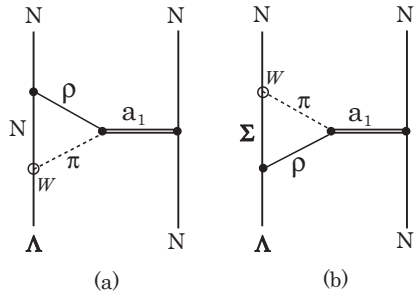

FIG. 1. The Feynman diagrams of $\rho\pi/a_1$ exchange process in which (a) contains a nucleon as the intermediate baryon and (b) a Σ as the intermediate baryon. The symbol W signifies the weak vertex.

The weak interaction Hamiltonians are adopted at the $\Lambda N\pi$ vertex and $\Sigma N\pi$ vertex in Figs. 1 and 2. They are the same as listed in Ref. [8]. Hamiltonians needed for the a_1-exchange potentials are given as follows:

$$H^S_{\rho\pi a_1} = g_{\rho\pi a_1}\boldsymbol{\phi}^{\mu}_{a_1}\cdot(\boldsymbol{\phi}_{\rho,\mu}\times\boldsymbol{\varphi}_{\pi}) + \text{h.c.} \tag{27}$$

$$H^S_{NNa_1} = g_{NNa_1}\bar{\psi}_N\gamma_5\gamma^{\mu}\boldsymbol{\tau}\psi_N\cdot\boldsymbol{\phi}_{a_1,\mu} - i\frac{f_{NNa_1}}{2M}\bar{\psi}_N(p')\gamma_5\sigma^{\mu\nu} \times(p'+p)_{\nu}\boldsymbol{\tau}\psi_N(p)\cdot\boldsymbol{\phi}_{a_1,\mu}(p'-p) + \text{h.c.} \tag{28}$$

$$H^S_{\Lambda\Sigma\rho} = g_{\Lambda\Sigma\rho}(\bar{\boldsymbol{\Psi}}_{\Sigma}\gamma^{\mu}\boldsymbol{\phi}_{\rho,\mu})\psi_{\Lambda} + \frac{f_{\Lambda\Sigma\rho}}{4M}[\bar{\boldsymbol{\Psi}}_{\Sigma}\sigma^{\mu\nu}\psi_{\Lambda} \times(\partial_{\mu}\boldsymbol{\phi}_{\rho,\nu} - \partial_{\nu}\boldsymbol{\phi}_{\rho,\mu})] + \text{h.c.} \tag{29}$$

$$H^S_{\sigma\pi a_1} = g_{\sigma\pi a_1}\boldsymbol{\phi}^{\mu}_{a_1}\cdot(\partial_{\mu}\phi_{\sigma}\boldsymbol{\varphi}_{\pi} - \phi_{\sigma}\partial_{\mu}\boldsymbol{\varphi}_{\pi}) + \text{h.c.}. \tag{30}$$

Other Hamiltonians are found in Ref. [8].

The coupling constants g_{NNa_1}, f_{NNa_1}, $g_{\Lambda\Sigma\rho}$, and $f_{\Lambda\Sigma\rho}$ are taken from the work of Rijken *et al.* [24,25]. We can evaluate $g_{\rho\pi a_1}$ from the decay width of the a_1 meson. The decay width of a_1 into $\rho+\pi$ is expressed in the form

$$\Gamma(a_1\to\rho\pi) = \frac{g^2_{\rho\pi a_1}}{4\pi}\frac{1}{m^2_{a_1}}\left[1+\frac{1}{3}\left(\frac{p}{m_{\rho}}\right)^2\right]p, \tag{31}$$

where p is an outgoing pion momentum, $p = 353$ MeV/c. The decay mode of a_1 into $\sigma+\pi$ is seen in the Particle Data Compilation [30]. The full width Γ is known to be 250–600 MeV. By assuming that the full width comes dominantly from the $a_1\to\rho\pi$ decay we evaluate $g_{\rho\pi a_1}$ from Eq. (31) as

$$\begin{aligned} g_{\rho\pi a_1} &= -4490\,\text{MeV} \sim -5500\,\text{MeV}, \text{ if} \\ \Gamma &= 400\,\text{MeV} \sim 600\,\text{MeV}. \end{aligned} \tag{32}$$

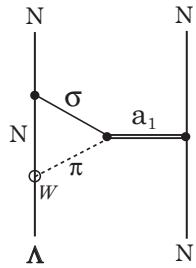

FIG. 2. The Feynman diagram of $\sigma\pi/a_1$ exchange process. The symbol W signifies the weak vertex.

We adopt a minus $(-)$ sign for $g_{\rho\pi a_1}$ which will be explained later.

The $g_{\sigma\pi a_1}$ is determined from considering the axial-vector current; namely the hadronic axial-vector current is coupled to the a_1 via the Lagrangian density as

$$L^{(A)}_I = 2g_A\left[\bar{\psi}_N\gamma_5\gamma^{\mu}\frac{\boldsymbol{\tau}}{2}\psi_N + (\partial^{\mu}\phi_{\sigma}\boldsymbol{\varphi}_{\pi} - \phi_{\sigma}\partial^{\mu}\boldsymbol{\varphi}_{\pi})\right]\cdot\boldsymbol{\phi}_{a_1,\mu}. \tag{33}$$

So, we take the relation,

$$g_{\sigma\pi a_1} = 2g_A = 2g_{NNa_1}. \tag{34}$$

Now, when one calculates the invariant amplitude $\mathcal{M}_{fi}(\Lambda N\to NN)$ of the $\rho\pi/a_1$ exchange diagrams in Figs. 1(a) and 1(b), one must evaluate the loop integral over the intermediate momentum k. After the Feynman integral is introduced, the loop integral has a form symbolically as

$$\int d^4kG(k) \tag{35}$$

and

$$G(k) = \frac{F_0+F_1k^2+F_2k^4}{[k^2-c]^3}. \tag{36}$$

This integral diverges at large k^2. To circumvent the divergence we introduce the regularization factor of the form

$$\left[\frac{\Lambda^2_n}{\boldsymbol{k}^2+\Lambda^2_n}\right]^n, \quad n=1,2. \tag{37}$$

The Λ_n's are parameters to be determined and $\boldsymbol{k}$ is a three-momentum.

We adopt at the NNa_1 vertex the form factor

$$FF = \frac{\Lambda^2_{a_1}}{\boldsymbol{q}^2+\Lambda^2_{a_1}}, \tag{38}$$

where $\boldsymbol{q} = \boldsymbol{p}'_1 - \boldsymbol{p}_{1\Lambda}$ is the momentum transfer and Λ_{a_1} is a cutoff mass.

The $\rho\pi/a_1(A)$ exchange potential $V_{\rho\pi/a_1(A)}$ is obtained as the Fourier transform of the invariant amplitude $i\mathcal{M}_{fi}$ for the diagram of Fig. 1(a). The parameters Λ_1 and Λ_2 and the coupling constant $g_{\rho\pi a_1}$ are determined in the following way. We construct the strong NN-force version from the similar $\rho\pi/a_1$ exchange diagram of $NN\to NN$ in which a Λ hyperon in Fig. 1(a) is replaced by a nucleon. We call it $V^{\text{strong}}_{\rho\pi/a_1}(NN-NN)$. Then we equate $V^{\text{strong}}_{\rho\pi/a_1}(NN-NN)$ approximately to $V^{\text{strong}}_{a_1}(NN-NN)$ of the a_1-exchange NN force of the ESC04 model [24] as

$$V^{\text{strong}}_{\rho\pi/a_1}(NN-NN) \approx V^{\text{strong}}_{a_1}(NN-NN). \tag{39}$$

The Λ_1, Λ_2, and $g_{\rho\pi a_1}$ are determined so that the approximate relation of Eq. (39) holds as well as possible. The potential $V_{\rho\pi/a_1(A)}$ is expressed in the isospin basis as

$$\begin{aligned} V_{\rho\pi/a_1(A)}(\boldsymbol{r}) = \{&V_S(r)(\boldsymbol{\sigma}_1\cdot\boldsymbol{\sigma}_2) + V_T(r)S_{12} \\ &+ V_{LS}(r)(\boldsymbol{L}\cdot\boldsymbol{S}) + iV_{V_1}(r)i[(\boldsymbol{\sigma}_1\times\boldsymbol{\sigma}_2)\cdot\hat{\boldsymbol{r}}] \\ &+ iV_{V_2}(r)(\boldsymbol{\sigma}_2\cdot\hat{\boldsymbol{r}})\}(\boldsymbol{\tau}_1\cdot\boldsymbol{\tau}_2). \end{aligned} \tag{40}$$

The particle 1 refers to a Λ hyperon. The parity-violating vector part of the potential is expressed in the imaginary form.

The $\rho\pi/a_1(B)$ exchange potential $V_{\rho\pi/a_1(B)}$ for the diagram depicted in Fig. 1(b) is evaluated in the same way as in the case of $V_{\rho\pi/a_1(A)}$ potential. The potential $V_{\rho\pi/a_1(B)}$ is expressed in the charge basis as

$$V_{\rho\pi/a_1(B)}(\boldsymbol{r}) = \{\text{same potential type except } (\boldsymbol{\tau}_1 \cdot \boldsymbol{\tau}_2) \text{ as in Eq. (40)}\}\mathcal{O}^T_{\rho\pi/a_1(B)}(\Lambda N \to NN). \quad (41)$$

The operator $\mathcal{O}^T$ refers to the isospin-dependent factor for the two-nucleon state, which reads

$$\mathcal{O}^T_{\rho\pi/a_1(B)}(\Lambda n \to nn) = 1 \quad (T=1), \quad (42)$$

$$\mathcal{O}^T_{\rho\pi/a_1(B)}(\Lambda p \to np) = -\frac{3}{\sqrt{2}} \quad (T=0), \qquad = \frac{1}{\sqrt{2}} \quad (T=1). \quad (43)$$

The explicit form of the potential terms in Eqs. (40) and (41) will be given elsewhere [31].

The $\sigma\pi/a_1$ exchange potential for the diagram of Fig. 2 is similarly evaluated. The loop integral of Fig. 2 has a similar form as Eq. (35) with

$$G(k) = \frac{F_{0s} + F_{1s}k^2}{(k^2 - c_s)^3}. \quad (44)$$

Because the integral diverges at large momentum k^2, we introduce the regularization factor of the form $\Lambda_1^2/(\boldsymbol{k}^2 + \Lambda_1^2)$, where Λ_1 is a parameter to be determined. The potential $V_{\sigma\pi/a_1}$ is expressed as

$$V_{\sigma\pi/a_1}(\boldsymbol{r}) = \{V_C(r) + V_S(r)(\boldsymbol{\sigma}_1 \cdot \boldsymbol{\sigma}_2) + V_T(r)S_{12} + V_{LS}(r)(\boldsymbol{L}\cdot\boldsymbol{S}) + iV_{V_1}(r)i[(\boldsymbol{\sigma}_1 \times \boldsymbol{\sigma}_2)\cdot\hat{\boldsymbol{r}}] + iV_{V_2}(r)(\boldsymbol{\sigma}_2\cdot\hat{\boldsymbol{r}})\}(\boldsymbol{\tau}_1\cdot\boldsymbol{\tau}_2). \quad (45)$$

Again, the explicit form of the potential terms in Eq. (45) will be given elsewhere [31].

The potentials of $V_{2\pi/\rho(A,B)}$ and $V_{2\pi/\sigma(A,B)}$ are modified from the previous version [8] in the following points. For the $V_{2\pi/\rho}$ potential, the $NN\rho$ vertex form factor of the $\Lambda_\rho^2/(\boldsymbol{q}^2 + \Lambda_\rho^2)$ type is introduced and the regularization factor of the $\Lambda_1^2/(\boldsymbol{k}^2 + \Lambda_1^2)$ type is employed in the loop integral of the intermediate momentum k. The ρ-meson mass $m_\rho = 771.1$ MeV is used and the coupling constant is a bit changed. For the $V_{2\pi/\sigma}$ potential, the $NN\sigma$ vertex form factor of the $(1 - \frac{\boldsymbol{q}^2}{M_X^2})\ \frac{\Lambda_\sigma^2}{\boldsymbol{q}^2+\Lambda_\sigma^2}$ type is introduced [24]. The first factor in the form factor has a zero at $\boldsymbol{q}^2 = M_X^2$, which reflects fact that the σ is internally a p-wave quark-antiquark state [24].

IV. RESULTS AND DISCUSSIONS

A. Features of a_1-meson exchange and total nonmesonic decay potential

The strong coupling constants and parameters adopted for the $\rho\pi/a_1$, $\sigma\pi/a_1$, $2\pi/\rho$, and $2\pi/\sigma$ exchange potentials are listed in Table I, where the coupling constants for the a_1 meson are taken from the ESC04 model [24,25]. We adopt the sign of g_{NNa_1} to be the same as that of $g_{NN\rho}$ and adopt also the sign of $g_{\rho\pi a_1}$ that of $g_{\pi\pi\rho}$, which are suggested from the chiral invariance argument by Schwinger [32]. Weak coupling constants and parameters are the same as those adopted in Ref. [8].

Three types of a_1-meson exchange potentials, $V_{\rho\pi/a_1(A)}$, $V_{\rho\pi/a_1(B)}$, and $V_{\sigma\pi/a_1}$, have been calculated. In the following, $V_{\rho\pi/a_1}$ means the addition of $V_{\rho\pi/a_1(A)}$ and $V_{\rho\pi/a_1(B)}$ potentials. The characteristic features of $V_{\rho\pi/a_1}$ are as follows: (i) the central and the tensor forces are strong at short range; (ii) the parity-violating force of the $i[(\boldsymbol{\sigma}_1 \times \boldsymbol{\sigma}_2)\cdot\hat{\boldsymbol{r}}]$ type is strong, whereas that of the $(\boldsymbol{\sigma}_2\cdot\hat{\boldsymbol{r}})$ type is weak; and (iii) the potentials $V_{\rho\pi/a_1(A)}$ and $V_{\rho\pi/a_1(B)}$ show almost similar r-dependent behavior though the former potential strength is quite a bit stronger than the latter. The potential features of $V_{\sigma\pi/a_1}$ are as follows: (i) the potential is dominantly of the central-force type and the potential strength is weak compared with that of the $\rho\pi/a_1$ exchange and (ii) the parity-violating forces are very weak.

Figure 3 shows the central-type $\Lambda p \to np$ transition potentials in the ${}^1S_0 \to {}^1S_0$ channel. Before introducing the a_1-meson exchange [8,9], the strongly positive $V_{2\pi/\sigma}$ determines the total potential behavior to be positive in the most effective region ($r \geqslant 0.5$ fm). It is remarkable here that the new potential of $V_{\rho\pi/a_1}$ is very strongly negative at the short range of $r \leqslant 1$ fm, which overwhelms the $V_{2\pi/\sigma}$ potential. The negative $V_{\sigma\pi/a_1}$ behaves additively. As a results, when the a_1-meson exchange is incorporated, the summed potential of ${}^1S_0 \to {}^1S_0$ channel is modified drastically to be strongly negative at the

TABLE I. Strong coupling constants and parameters adopted in the $\rho\pi/a_1$, $\sigma\pi/a_1$, $2\pi/\rho$, and $2\pi/\sigma$ exchange potentials.

$g_{NNa_1} = 8.5893$	$f_{NNa_1} = 0.0$	
$g_{\Lambda\Sigma\rho} = 0.0$	$f_{\Lambda\Sigma\rho} = 7.6719$	
$g_{\rho\pi a_1} = -5020$ MeV	$m_{a_1} = 1230.0$ MeV	$\Lambda_{a_1} = 1400$ MeV
$\Lambda_1(\rho\pi/a_1) = 2000$ MeV	$\Lambda_2(\rho\pi/a_1) = 1650$ MeV	
$g_{NN\sigma} = 6.30$	$g_{\sigma\pi a_1} = 17.1786$	$\Lambda_1(\sigma\pi/a_1) = 1500$ MeV
$g_{NN\rho} = 2.9870$	$f_{NN\rho} = 14.7557$	
$g_{\Lambda\Sigma\pi} = 7.66$	$g_{\pi\pi\rho} = -8.0$	$m_\rho = 771.1$ MeV
$\Lambda_\rho = 900$ MeV	$\Lambda_1(2\pi/\rho) = 920$ MeV	
$g_{\pi\pi\sigma} = -1850$ MeV	$m_\sigma = 600.0$ MeV	
$\Lambda_\sigma = 1130$ MeV	$M_X = 760$ MeV	

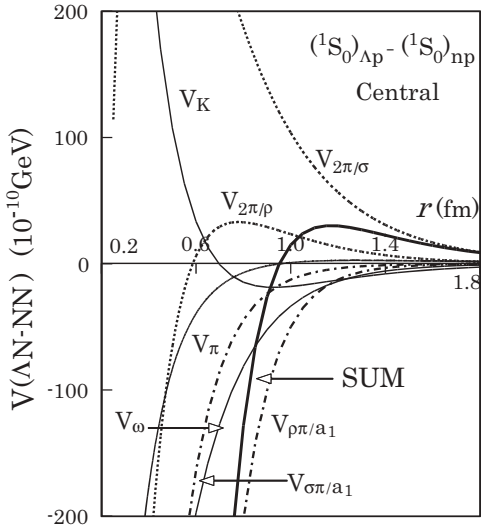

FIG. 3. The central-type weak transition potentials for various meson and meson-pair exchanges in the $(^1S_0)_{\Lambda p} \to (^1S_0)_{np}$ channel. The thin solid lines correspond to the π, ω, and K exchanges, whereas the dotted lines to the $2\pi/\sigma$ and $2\pi/\rho$ exchanges. The a_1-meson exchange potentials are depicted by dash-dot lines, and the summed transition potential is shown by the thick solid line.

short range region. The individual potentials in the $^3S_1 \to {}^3S_1$ channel (not shown here) behave almost similarly as the corresponding ones in the $^1S_0 \to {}^1S_0$ channel. Therefore, the summed potential for the $^3S_1 \to {}^3S_1$ channel is also modified to be strongly negative at short range.

Figure 4 shows the tensor potentials in the $^3S_1 \to {}^3D_1$ channel for the various meson exchanges. The $V_{\rho\pi/a_1}$ is strongly positive at short range in contrast to $V_{2\pi/\rho}$. The $V_{\sigma\pi/a_1}$ has almost no contribution. As a result, when the a_1-meson exchange is considered, the summed potential in this tensor channel changes its behavior drastically. The summed potential

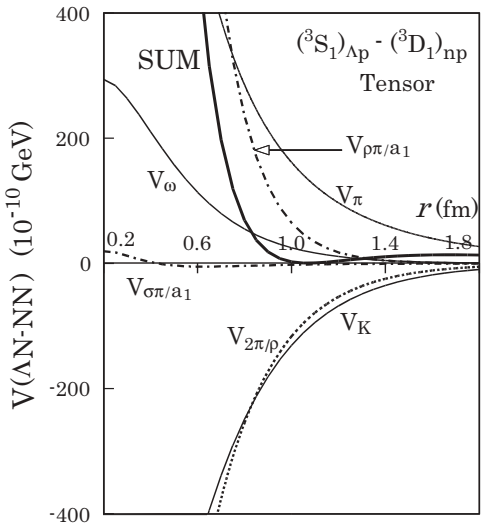

FIG. 4. The tensor-type weak transition potentials for various meson and meson-pair exchanges in the $(^3S_1)_{\Lambda p} \to (^3D_1)_{np}$ channel. See also the caption to Fig. 3.

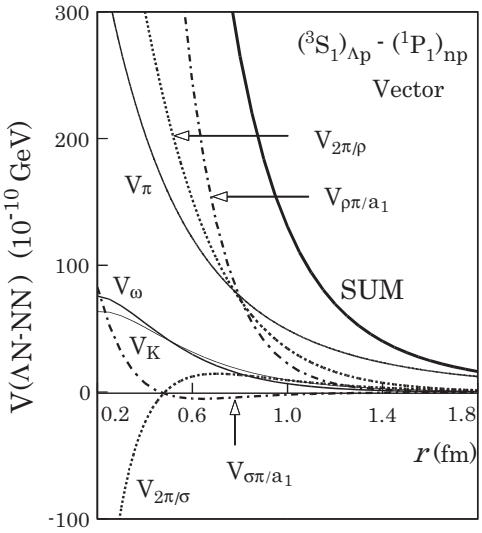

FIG. 5. The parity-violating vector-type weak transition potentials for various meson and meson-pair exchanges in the $(^3S_1)_{\Lambda p} \to (^1P_1)_{np}$ channel. See also the caption to Fig. 3.

is almost vanishing at $r \geqslant 0.9$ fm and changes its sign to be positive at the shorter range. This behavior is quite different from the case of our previous $\pi + 2\pi/\rho + 2\pi/\sigma + \omega + K$ exchange model.

Figure 5 shows the parity-violating vector potentials in the $^3S_1 \to {}^1P_1$ channel. The $V_{\rho\pi/a_1}$ potential of the $i[(\boldsymbol{\sigma}_1 \times \boldsymbol{\sigma}_2) \cdot \hat{\boldsymbol{r}}]$ type contributes strongly with a positive sign, which behaves additively to $V_{2\pi/\rho}$. The $(\boldsymbol{\sigma}_2 \cdot \hat{\boldsymbol{r}})$-type potential does not contribute as much. The summed potential stays strongly positive and is enlarged. In the other parity-violating channels, $^1S_0 \to {}^3P_0$ and $^3S_1 \to {}^3P_1$, the a_1-meson exchange does not produce large effects.

It is appropriate to note the typical contributions of the chiral partner mesons, π vs. σ and ρ vs. a_1, to the transition potential. It is well known that π exchange produces a strong tensor force, whereas σ exchange ($2\pi/\sigma$ exchange in our model) produces a strong central one as seen in Figs. 4 and 3. The central force of $2\pi/\rho$ exchange is weak, whereas that of $\rho\pi/a_1$ exchange is strong enough at short distances. Another feature is that the tensor forces from $2\pi/\rho$ exchange and $\rho\pi/a_1$ exchange have similar strength but completely opposite signs at short distances. The parity-violating potentials for the $2\pi/\rho$ and $\rho\pi/a_1$ exchanges work additively. From these observations, we recognize that it is very important to take the mesonic chiral partners into account simultaneously in evaluating the transition potential. In this respect, an extension of the study of chirality to the strange-meson sector, including κ, K, and K^*, might be a forthcoming subject toward a refinement of the present model.

B. Nonmesonic decay rates and asymmetry parameter of ${}^5_\Lambda$He

The nonmesonic weak decay rates and the asymmetry parameters are evaluated for the light Λ hypernuclei as ${}^5_\Lambda$He, ${}^{11}_\Lambda$B, and ${}^{12}_\Lambda$C in the shell-model framework. It is known from the reaction analyses for (π^+, K^+) and (K^-, π^-) that

these hypernuclei are well described [27] by the product wave functions as shown by Eq. (7).

In evaluating the $\Lambda N \to NN$ transition matrix element, the initial state correlation for ΛN and the final state correlation for the outgoing NN are carefully taken into account. See Ref. [8] for details. Then the ΛN wave function $\phi_{n\ell}(r)\mathcal{Y}_{\ell S\mathcal{J}}$ in Eq. (23) is replaced as

$$\phi_{n0}(r)\mathcal{Y}_{0SS} \to f_S(r)\phi_{n0}(r)\mathcal{Y}_{0SS} + \delta_{S1} f_2(r)\mathcal{Y}_{211} \qquad (46)$$

for the relative $s(\ell = 0)$ wave. The $f_S(r)$ is a correlation function for the s wave and f_2 is the induced d wave. The relative $p(\ell = 1)$ wave contribution is small and is not considered in the present work. The final state $j_{\ell_0}(k, r)\mathcal{Y}_{\ell_0 S'_2\mathcal{J}}$ in Eq. (23) is replaced by the scattering state as

$$i^{\ell_0} j_{\ell_0}(k, r)\mathcal{Y}_{\ell_0 S'_2\mathcal{J}} \to i^{\ell_0}\psi_{\ell_0 S'_2\mathcal{J}}(k, r)\mathcal{Y}_{\ell_0 S'_2\mathcal{J}} + \delta_{S'_2 1}\delta_{\mathcal{J}1}\left[\delta_{\ell_0 0} i^2 \chi_2(k, r)\mathcal{Y}_{211} + \delta_{\ell_0 2} i^0 \chi_0(k, r)\mathcal{Y}_{011}\right]. \qquad (47)$$

The $\psi_{\ell_0 S'_2\mathcal{J}}$ is the scattering wave and the χ_2 and χ_0 are the induced d and s waves, respectively, due to the NN tensor interaction.

Table II lists the calculated results for ${}^{5}_{\Lambda}$He together with the experimental data. In the $\pi + 2\pi/\rho + 2\pi/\sigma + \omega + K$ exchange model the n/p ratio is enhanced strongly mainly due to π- and K-meson exchanges [9,11,12,14], although the theoretical Γ_n/Γ_p seems too large. Note that the a_1-meson exchange gives rise to a much better n/p ratio (0.508) to be really comparable with the recent experimental data [4,5].

One of the most important results of the a_1-exchange mechanism is that this can naturally give a small asymmetry parameter $\alpha_\Lambda = 0.083$ in good agreement with the recent high-quality data [1,4,5]. This shows the most drastic change, because the previous calculation without a_1-meson exchange gives $\alpha_\Lambda = -0.833$ as compared in Table II. To confirm this novel result, we discuss the detailed reason for the change below.

For the present purpose it is illuminating to refer to the expression of the asymmetry parameter in the nonmesonic decay from a polarized "free" Λ hyperon:

$$\alpha_{\Lambda(\text{free})} = \frac{2\sqrt{3}\,\text{Re}[-ae^* + b(c - \sqrt{2}d)^*/\sqrt{3} + f(\sqrt{2}c + d)^*]}{|a|^2 + |b|^2 + 3[|c|^2 + |d|^2 + |e|^2 + |f|^2]}. \qquad (48)$$

The numerator Γ_1 of α_Λ for ${}^{5}_{\Lambda}$He contains the similar expression as that of Eq. (48), which is understood in Eq. (20) if one realizes $\cos\theta_k \approx -1$, because the opening angle $\theta_k \approx 180^\circ$ contributes dominantly in the nonmesonic decay. However, one should bear in mind that the amplitudes a, b, c, d, e, and f in Eq. (20) are supplemented by the structure factors and are integrated.

In the previous calculation within the $\pi + 2\pi/\rho + 2\pi/\sigma + \omega + K$ exchange model, the large and negative value ($\alpha_\Lambda = -0.833$) comes dominantly from the $-ae^*$ term and next from the $\sqrt{2}fc^*$ term. In this model, both amplitudes a and e are large with a positive sign, which leads $-ae^*$ to be negative and large. The positive and large value of the a amplitude is mainly due to the $2\pi/\sigma$ exchange potential, which is overwhelmingly strong with a positive sign in the ${}^1S_0 \to {}^1S_0$ channel. The amplitude e is known to be positive and strong because most of the meson exchange potentials contribute additively with a positive sign in the ${}^3S_1 \to {}^1P_1$ channel. The $\sqrt{2}fc^*$ factor is definitely negative, because f is negative and c is positive. It is noted here that the amplitude c has contributions from ${}^3S_1 \to {}^3S_1$ (direct amplitude c_0) and also from ${}^3S_1 \to$ induced-${}^3D_1$ channels (induced amplitude $\tilde{d}$) due to the final-state tensor correlation as explained in Eq. (47); that is, $c = c_0 + \tilde{d}$. Although the summed potential of the direct channel and that of the induced channel have opposite signs, the two channel contributions work additively owing to the phase factor $i^{\ell'_0}$ and $\ell'_0 = 0$ and 2. Likewise, the d amplitude is composed of the direct d_0 and the induced $\tilde{c}$ amplitudes, i.e., $d = d_0 + \tilde{c}$. In this way we have a large and negative value ($\alpha_\Lambda = -0.833$) in the $\pi + 2\pi/\rho + 2\pi/\sigma + \omega + K$ exchange model.

However, when the a_1-meson exchange interaction is introduced, $\rho\pi/a_1$ and $\sigma\pi/a_1$ exchange central potentials work together to modify the inner radial behavior of the summed potentials in the ${}^1S_0 \to {}^1S_0$ and ${}^3S_1 \to {}^3S_1$ channels. See Fig. 3 for the ${}^1S_0 \to {}^1S_0$ channel. The tensor force of the $\rho\pi/a_1$ exchange has a vital role to cancel the tensor force of $2\pi/\rho$ exchange potential as is noted in Sec. IV A and leads to a modification of the summed potential as seen in Fig. 4. In the ${}^3S_1 \to {}^1P_1$ channel the $\rho\pi/a_1$ exchange works to enlarge the summed potential in Fig. 5. As a result, the $-ae^*$ term turns out to be positive. The combination $f(\sqrt{2}c + d)^*$ remains, however, negative, because fd^* is negative and dominates over $\sqrt{2}fc^*$. The $b(c - \sqrt{2}d)^*/\sqrt{3}$ term contribution is small and positive. Finally, such cancellation gives rise to a very small α_Λ.

The calculated decay rate Γ_{nm} is 0.358, which is 16% smaller than the experimental data of Ref. [1]. The two-nucleon induced decay process [33] might explain some part of this discrepancy.

TABLE II. Calculated decay rates, Γ_n/Γ_p ratios, and the asymmetry parameters of ${}^{5}_{\Lambda}$He in the three meson-exchange models are compared with the experimental data. The decay rates are shown in units of the free Λ decay rate Γ_Λ.

	Γ_{nm}	Γ_n/Γ_p	$\alpha_\Lambda = \alpha_1$
π	0.278	0.109	-0.417
$\pi + 2\pi/\rho + 2\pi/\sigma + \omega + K$	0.379	0.707	-0.833
$\pi + 2\pi/\rho + 2\pi/\sigma + \omega + K + \rho\pi/a_1 + \sigma\pi/a_1$	0.358	0.508	0.083
Exp. [1,2,4]	0.424 ± 0.024	$0.45 \pm 0.11 \pm 0.03$	$0.11 \pm 0.08 \pm 0.04$
Exp. [5]			$0.07 \pm 0.08^{+0.08}_{-0.00}$
Exp. [6]			0.24 ± 0.22

TABLE III. Parameter sets, Set A to Set E, of cutoff masses in the form factors and the coupling constants in evaluating the $\rho\pi/a_1$- and $\sigma\pi/a_1$-exchange transition potentials. Parameters are given in units of MeV except $g_{\sigma\pi a_1}$.

	Set A	Set B	Set C	Set D	Set E
Λ_{a_1}	1400	1400	1400	1100	1600
$\Lambda_1(\rho\pi/a_1)$	2000	1650	2000	2000	2000
$\Lambda_2(\rho\pi/a_1)$	1650	1650	2000	1650	1650
$g_{\rho\pi a_1}$	−5020	−5020	−5020	−4000	−5020
$\Lambda_1(\sigma\pi/a_1)$	1500	1500	1500	1500	1500
$g_{\sigma\pi a_1}$	17.18	17.18	17.18	17.18	17.18

Before going to the ${}^{12}_{\Lambda}$C and ${}^{11}_{\Lambda}$B cases, it is interesting to examine the sensitivity of the decay observables to the a_1-meson exchange potential parameters such as the cutoff masses and the coupling constants. Here we have five options of the parameters as listed in Table III. The $g_{NNa_1} = 8.5893$ is commonly used. As already mentioned together with Table I, the "standard" choice of the parameters based on the relation of Eq. (39) is denoted as Set A in Table III. Then we change three cutoff masses Λ_{a_1} in the NNa_1 vertex form factor of Eq. (38) within acceptable ranges and select four other combinations (Set B to Set E) as listed in Table III. It is noted that the monopole-type form factor of Eq. (38) with cutoff $\Lambda_{a_1} = 1400$ MeV (1100 MeV, 1600 MeV) simulates well the Gaussian form factor of $\exp[-\boldsymbol{q}^2/\Lambda^2]$ with $\Lambda = 1450$ MeV (1150 MeV, 1650 MeV) at $q \simeq 300$–$600\,\mathrm{MeV}/c$, which is the most relevant region of momentum transfer in the nonmesonic decay. The following behavior of the potential is noticed. When the smaller cutoff Λ_{a_1} is adopted, the potential strength is naturally reduced at the region less than $r \approx \hbar/\Lambda_{a_1}c$, whereas at larger distances up to $r \sim 1$ fm the reduction becomes milder in comparison with the case of adopting the bigger Λ_{a_1}. Due to such a potential behavior, the coupling constant $g_{\rho\pi a_1} = -4000$ MeV is chosen in Set D to meet the relation of Eq. (39) at $r \geqslant 0.5$ fm.

The calculations of the decay rates and the asymmetry parameter of ${}^{5}_{\Lambda}$He are performed also with these options of Set B to Set E. In Table IV we compare the calculated results for ${}^{5}_{\Lambda}$He for the five parameter sets, A–E, of Table III. One sees in Table IV that the calculated asymmetry parameter α_Λ is sensitive to the cutoff Λ_{a_1} used in the potentials, though the decay rates are not so changed. Because the cutoff masses as Λ_{a_1}, $\Lambda_1(\rho\pi/a_1)$, $\Lambda_2(\rho\pi/a_1)$, and $\Lambda_1(\sigma\pi/a_1)$ control the short-range behavior of the a_1-exchange potentials, it is natural that the asymmetry parameter α_Λ depends sensitively on the signs and magnitudes of the summed potentials. Thus the α_Λ might give us subtle information on the behavior of the weak decay potentials especially at the short distance. Within the present model framework it seems reasonable to adopt the parameter Set A for the $\rho\pi/a_1$ and $\sigma\pi/a_1$ exchange potentials.

TABLE IV. Calculated numbers of decay observables of ${}^{5}_{\Lambda}$He for the various parameter sets listed in Table III of the a_1-meson exchange potentials. The decay rates are shown in units of the free Λ decay rate Γ_Λ.

	Γ_p	Γ_n	Γ_{nm}	Γ_n/Γ_p	α_Λ
Set A	0.237	0.121	0.358	0.508	0.083
Set B	0.233	0.118	0.352	0.508	0.121
Set C	0.261	0.127	0.388	0.484	0.413
Set D	0.257	0.127	0.354	0.497	0.414
Set E	0.227	0.118	0.344	0.518	−0.167

C. Nonmesonic decay rates and asymmetry parameters of ${}^{12}_{\Lambda}$C and ${}^{11}_{\Lambda}$B

Table V summarizes the results for ${}^{12}_{\Lambda}$C. In the $\pi + 2\pi/\rho + 2\pi/\sigma + \omega + K$ exchange model, the Γ_n/Γ_p ratio is large compared with the recent experimental data [1,3]. The calculated proton asymmetry parameter α_1 of ${}^{12}_{\Lambda}$C is 0.377, which is equivalent to the intrinsic asymmetry parameter $\alpha_\Lambda = -0.755$. This value deviates from the experiment [1,4,5] very much. In contrast to these results, when the a_1-meson exchange is introduced, the Γ_n/Γ_p ratio is improved to the value of 0.407 and the intrinsic asymmetry parameter α_Λ is dramatically changed to be 0.045. These new theoretical values are both well comparable with the recent experimental data [4,5]. The decay rate Γ_{nm} is calculated to be 0.754, which is a little smaller than the experiment [1,34] but still within the error bars.

Table VI shows the calculated results for ${}^{11}_{\Lambda}$B with $J_H = 5/2^+$ together with the available experimental data. The general trends of the calculations for ${}^{11}_{\Lambda}$B are very similar to those for ${}^{12}_{\Lambda}$C especially for the Γ_n/Γ_p rations and the asymmetry parameters α_Λ. It is noted particularly for ${}^{11}_{\Lambda}$B that in the evaluation of Γ_1 of Eq. (A1) in the Appendix, the sum for the angular momentum L_0 extends $L_0 = 0$ and 2, when the nucleon in the orbit $(n_a \ell_a j_a) = 0p_{3/2}$ contributes to the nonmesonic decay rate. The contribution of the $L_0 = 2$ part to Γ_1 is, however, as small as 2% of the contribution of $L_0 = 0$ part to Γ_1. The calculated α_Λ is 0.078, which is in agreement within error bars with the averaged decay data of ${}^{12}_{\Lambda}$C and ${}^{11}_{\Lambda}$B hypernuclei [4,5].

It is worth to mention that the calculated intrinsic asymmetry parameters for light ${}^{5}_{\Lambda}$He, ${}^{11}_{\Lambda}$B and ${}^{12}_{\Lambda}$C hypernuclei have very similar numbers, though the numbers should have some uncertainties because of the approximations adopted in the derivations of the decay potentials and also of the simple wave functions used. It can also be noted that the recent experimental data of α_Λ [4–6] for those light Λ hypernuclei have small values with common overlaps within error bars.

In view of these observations, we note that the intrinsic asymmetry parameter α_Λ is a "good" observable that gives us direct and subtle information of the $\Lambda + p \to n + p$ transition interaction at short range. Naturally it does not depend much on the detailed hypernuclear structures, spins, and hypernuclear species [6].

The present results have demonstrated an essential role, in the context of our model, of the a_1 exchanges in explaining the observed small α_Λ. As mentioned, it was difficult to get small α_Λ in our previous calculations [9] and also in the present work in which the $\pi + 2\pi/\rho + 2\pi/\sigma + \omega + K$ exchange model

TABLE V. Calculated decay rates, Γ_n/Γ_p ratios and the asymmetry parameters of ${}^{12}_{\Lambda}$C in the three meson-exchange models are compared with the experimental data. The decay rates are shown in units of the free Λ decay rate Γ_Λ.

	Γ_{nm}	Γ_n/Γ_p	$\alpha_\Lambda = -\frac{J_H+1}{J_H}\alpha_1$
π	0.620	0.101	-0.340
$\pi + 2\pi/\rho + 2\pi/\sigma + \omega + K$	0.843	0.618	-0.755
$\pi + 2\pi/\rho + 2\pi/\sigma + \omega + K + \rho\pi/a_1 + \sigma\pi/a_1$	0.754	0.407	0.045
Exp. [1,4]	0.940 ± 0.035	$0.56 \pm 0.12 \pm 0.04$	$-0.20 \pm 0.26 \pm 0.04$
Exp. [5]			$-0.16 \pm 0.28^{+0.18}_{-0.00}$
Exp. [3]		$0.51 \pm 0.13 \pm 0.05$	
Exp. [34]	$0.824 \pm 0.056 \pm 0.066$		

has been applied. In this connection, we recall the article by Chumillas *et al.* [22], who claimed that the α_Λ of ${}^{5}_{\Lambda}$He, ${}^{12}_{\Lambda}$C, and ${}^{11}_{\Lambda}$B can be explained well within the octet-meson exchange potentials and the correlated $2\pi(2\pi/\sigma)$ + uncorrelated 2π exchange potentials calculated by Jido *et al.* [11]. Their conclusion seems different from that of our calculation. Note that our $2\pi/\sigma$ exchange interaction is regarded to be an effective potential that contains also uncorrelated 2π exchange contributions to some extent in addition to the correlated ones. In fact the $2\pi/\sigma$ exchange NN force of our model is quite similar to the NN force in Fig. 14 of Ref. [11]. However, it is not always easy to make a direct comparison between these two approaches. Moreover, the intermediate baryons adopted in the calculation of the weak $\Lambda N \to NN$ force are also different: NN and $N\Delta$ channels are considered but ΣN channel is not in Refs. [11,22], whereas in our model [7–9] the intermediate baryons N and Σ are taken into account but Δ, at least explicitly, is not.

V. SUMMARY AND OUTLOOK

The recent high-quality experiments for hypernuclear nonmesonic weak decays provided us with a converging value of Γ_n/Γ_p ratio $\simeq$0.5. This value deviates much from the basic one-pion-exchange mechanism, and therefore many theoretical efforts have been made for the explanation. Another important observable is the asymmetry parameter α_Λ of protons emitted in the decay, and the observed values now tend to be very small, differing from almost all the theoretical estimates. Thus how to understand these experimental data consistently from the viewpoint of meson-exchange models for the $\Lambda N \to NN$ weak transition interaction has been a long-standing dispute.

To give an answer to the challenging questions mentioned above, we have introduced the axial-vector a_1-meson exchange, for the first time, into the estimate of the ΛN weak interaction. The chief argument is to investigate the short-range properties of the weak interaction and, for that purpose, to make the set of exchanged mesonic quantum numbers more complete. It is noted, moreover, that the a_1 meson is the chiral partner of the ρ meson. Furthermore, the introduction of this new mechanism was stimulated by the success of the ESC04 model for the strong baryon-baryon interactions. The a_1-meson exchange has been treated in the form of $\rho\pi/a_1$ and $\sigma\pi/a_1$ combinations within the meson-pair exchange framework.

We have presented the calculated results for ${}^{5}_{\Lambda}$He, ${}^{11}_{\Lambda}$B, and ${}^{12}_{\Lambda}$C in the $\pi + 2\pi/\rho + 2\pi/\sigma + \omega + K + \rho\pi/a_1 + \sigma\pi/a_1$ exchange interaction model. The results are also compared with the estimates without the a_1-meson exchange. First, we have found the striking role of a_1 exchange in giving rise to remarkable modifications of the parity-conserving decay potentials (${}^{1,3}S \to {}^{1,3}S$ and ${}^{3}S_1 \to {}^{3}D_1$) at short range $r \leqslant 1$ fm.

Second, as a direct result of the short-range behavior mentioned above, we obtained a drastic change in the estimate of the intrinsic asymmetry parameter α_Λ, and the value for ${}^{5}_{\Lambda}$He becomes very small and positive (0.08) in good agreement with the recent high-quality experimental data. One notices that the intrinsic asymmetry parameters do not change much for other species: $\alpha_\Lambda = 0.08$ and 0.04 for ${}^{11}_{\Lambda}$B and ${}^{12}_{\Lambda}$C, respectively. These theoretical values of α_Λ compare well with the observed value, being essentially zero within the experimental error bars.

TABLE VI. Calculated decay rates, Γ_n/Γ_p ratios and the asymmetry parameters of ${}^{11}_{\Lambda}$B in the three meson-exchange models are compared with the experimental data. The decay rates are shown in units of the free Λ decay rate Γ_Λ.

	Γ_{nm}	Γ_n/Γ_p	$\alpha_\Lambda = -\frac{J_H+1}{J_H}\alpha_1$
π	0.519	0.123	-0.289
$\pi + 2\pi/\rho + 2\pi/\sigma + \omega + K$	0.760	0.732	-0.869
$\pi + 2\pi/\rho + 2\pi/\sigma + \omega + K + \rho\pi/a_1 + \sigma\pi/a_1$	0.660	0.503	0.078
Exp. [34]	$0.861 \pm 0.063 \pm 0.073$		
Exp. [4]			$-0.20 \pm 0.26 \pm 0.04$
Exp. [5]			$-0.16 \pm 0.28^{+0.18}_{-0.00}$

Additionally we have tried to vary the cutoff-mass parameters within acceptable ranges and found that the theoretical α_Λ is rather sensitive to their choice, although we think the essential role of the a_1-meson exchange is persistent. For the theoretical calculation of $\alpha_1 = \Gamma_1/\Gamma_0$ (or α_Λ), which comes from the interference between parity-conserving and parity-violating terms, one should be careful in treating the phases concerned. For this purpose we present the general expression of the proton asymmetry in the outgoing proton helicity frame.

As the third point, we emphasize that the inclusion of the a_1 meson improves the Γ_n/Γ_p ratios such as to become well comparable to the experimental data of ${}^{5}_{\Lambda}$He and ${}^{12}_{\Lambda}$C. Thus, in this article, we have shown the unique and important role that a_1 exchange can play when added to the nonmesonic weak decay interaction, noting that it leads to a consistent explanation for the existing experimental data of light Λ-hypernuclear decays ($A \leqslant 12$).

We make several remarks on the underlying behaviors of the $\Lambda N \to NN$ weak potentials obtained here from various meson- and meson-pair exchange mechanisms. The $\rho\pi/a_1$ exchange potential is short range in nature and has notable features in the central and tensor forces and the parity-violating vector force of the $i[(\boldsymbol{\sigma}_1 \times \boldsymbol{\sigma}_2)\cdot\hat{\boldsymbol{r}}]$ type. The a_1-exchange central force is strong enough (negative sign) to cancel out the $2\pi/\sigma$ exchange central force. The tensor force is strong (positive sign) and behaves in opposition to that of the $2\pi/\rho$ exchange one. The parity-violating force in the ${}^3S_1 \to {}^1P_1$ channel is strong and works additively to other meson-exchange interactions. The $\sigma\pi/a_1$-exchange potential is dominantly of the central type but the effect is relatively small. Such potential behaviors due to the a_1-meson exchange are the reason for the remarkable changes in α_Λ and Γ_n/Γ_p.

The present study is the first extension of the previous work in Ref. [8] through the proper consideration of the chiral partners in meson exchanges in the non-strange-meson sector and the introduction of the K-meson exchange. Although we are successful at present in explaining the weak decay observables of light Λ hypernuclei, further elaboration of the theoretical basis is interesting. Because the nonmesonic weak decay is a high-momentum-transfer process, short-range properties of the weak transition potentials should be further explored through the exchanges of chiral partnership mesons extending to the strange-meson sector. As another direction of sophistication, the short-range behaviors of the initial-ΛN and final-NN states should be solved with the aid of the modern soft-core baryon-baryon interactions in place of the hard-core strong interaction [35] employed in the present treatment. Naturally such improvement along these directions are planned in the next stage.

ACKNOWLEDGMENTS

The authors thank Y. Yamamoto for offering us the initial ΛN state correlation functions together with useful comments. They are grateful to T. Nagae, T. Maruta, T. Kishimoto, S. Ajimura, and E. Hiyama for their interests and discussions. This work has been done under the support of Grant-in-Aid for Scientific Research (Grant no. 13640294) and Grant-in-Aid for Scientific Research in Priority Area (Multi-Quark System Probed by Strangeness, Grant no. 18042005) from Ministry of Education, Culture, Sports, Science and Technology of Japan.

APPENDIX: EXPRESSION OF Γ_1 DEFINED BY EQ. (3)

The Γ_1 shown generally by Eq. (11) is expressed in terms of the two-body transition amplitudes and in the case of ΛN relative s wave in the shell-model framework as

$$
\begin{aligned}
\Gamma_1 = {} & \frac{2\pi}{2J_H+1} \times 2M_N \times \frac{3}{J_H+1} \sum_{J'_1 M'_1 \alpha'_1} \sum_{T'_1 M_{T'_1}} \sum_{T'_2 M_{T'_{22}}} \sum_{J_2 M_2} \sum_{J_{22}} \\
& \times \sum_{M_{H_0}>0} \sum_{\ell_a j_a} \sum_{\ell'_a j'_a} \frac{1}{(2\pi)^6} \int d(\cos\theta_{k_1}) d\phi_{k_1} \int_0^{k_2^{\max}} dk_2 \\
& \times \frac{(A-2)k_1^2 k_2^2}{\sqrt{(A-1)(A-2)k_Q^2 - k_2^2[(A-1)^2 - \cos^2\theta_{k_1}]}} \\
& \times \left(4\pi\right)^2 (T'_1 M_{T'_1} 1/2 v_p | T_H M_{T_H})^2 (-1)^{\ell_a + j_a + j_\Lambda} \\
& \times (-1)^{\ell'_a + j'_a + j_\Lambda} \mathcal{S}^{1/2}_{J_c T_c, J'_1 T'_1 \alpha'_1}(j_a, t_N = 1/2) \mathcal{S}^{1/2}_{J_c T_c, J'_1 T'_1 \alpha'_1} \\
& \times (j'_a, t_N = 1/2) \sqrt{(2J_c+1)(2J_2+1)} W(J'_1 j_a J_H j_\Lambda; \\
& \times J_c J_2) \sqrt{(2J_c+1)(2J_{22}+1)} W(J'_1 j'_a J_H j_\Lambda; J_c J_{22}) \\
& \times \left(J'_1 M'_1 J_2 M_2 | J_H M_{H_0}\right)\left(J'_1 M'_1 J_{22} M_2 | J_H M_{H_0}\right) \times M_{H_0} \\
& \times \sum_{S=\mathcal{J}} \sum_{S'=\mathcal{J}'} \sqrt{(2j_a+1)(2S+1)} W(j_a \ell_a j_\Lambda S; 1/2 J_2) \\
& \times \sqrt{(2j'_a+1)(2S'+1)} W(j'_a \ell'_a j_\Lambda S'; 1/2 J_{22}) \\
& \times \sum_{nN} \sum_{n'N'} \sum_{n_\Lambda n'_\Lambda} (-1)^{L-\lambda} M_{\lambda=\ell_a=L}(n_a \ell_a n_\Lambda 0; n 0 N L; \\
& \times M_N, M_\Lambda) c(n_\Lambda) (-1)^{L'-\lambda'} M_{\lambda'=\ell'_a=L'}(n'_a \ell'_a n'_\Lambda 0; \\
& \times n' 0 N' L'; M_N, M_\Lambda) c(n'_\Lambda) (2\pi)^3 (-1)^{N+N'} (-i)^{L-L'} \\
& \times \phi_{NL}\left(K, \frac{1}{b_R}\right) \phi_{N'L'}\left(K, \frac{1}{b_R}\right) \sum_{\mathcal{M}\mathcal{M}'} \sum_{M M'} (\mathcal{J}\mathcal{M} L M | J_2 M_2) \\
& \times (\mathcal{J}'\mathcal{M}' L' M' | J_{22} M_2) \times (-1)^{M_2} \sum_k \sum_{L_0} \\
& \times \sqrt{\frac{(2\mathcal{J}+1)(2\mathcal{J}'+1)}{2k+1}} (-1)^k (\mathcal{J}\mathcal{M}\mathcal{J}' - \mathcal{M}' | k \mathcal{M} \\
& - \mathcal{M}') \sqrt{\frac{(2L+1)(2L'+1)}{4\pi}} (L M L' - M' | L_0 M - M') \\
& \times (L 0 L' 0 \mid L_0 0) Y_{k, \mathcal{M}-\mathcal{M}'}(\theta_k, \phi_k) Y_{L_0, M-M'}(\theta_K, \phi_K) \\
& \times \sum_{S'_2} \sum_{\ell_0} \sum_{\ell'_0} \sqrt{\frac{(2\ell_0+1)(2\ell_0'+1)}{4\pi}} (-1)^{S'_2} 2 \\
& \times \left[\frac{1 - (-1)^k (-1)^{L-L'}}{2}\right] W(\mathcal{J}\ell_0 \mathcal{J}' \ell'_0; S'_2 k)(\ell_0 0 \ell'_0 0 | k 0) \\
& \times \left\langle i^{\ell_0} j_{\ell_0}(k, r) \mathcal{Y}_{\ell_0 S'_2 \mathcal{J}} \xi^{T'_2}_{\nu_p + 1/2} \right| V_{nm}(\Lambda N - N N) \left| \phi_{n, \ell=0} \right. \\
& \times \mathcal{Y}_{\ell=0 S \mathcal{J}=S} \xi^{T_2=1/2}_{\nu_p} \left\rangle \right\langle i^{\ell'_0} j_{\ell'_0}(k, r) \mathcal{Y}_{\ell'_0 S'_2 \mathcal{J}'} \xi^{T'_{22}}_{\nu_p + 1/2} \left| V_{nm}(\Lambda N \right. \\
& - N N) \left| \phi_{n', \ell'=0} \mathcal{Y}_{\ell'=0 S' \mathcal{J}'=S'} \xi^{T_{22}=1/2}_{\nu_p} \right\rangle^*. \qquad \text{(A1)}
\end{aligned}
$$

Here $M_\lambda(n_a\ell_a n_\Lambda\ell_\Lambda; n\ell NL; M_N, M_\Lambda)$ is a generalized Talmi-Moshinsky transformation coefficient for different masses of a nucleon and a Λ hyperon. Other notations used are the same as those in Ref. [8].

When the nonmesonic decay takes place from the ΛN relative s state, the angular momentum k takes 1 only and L_0 must have even number, 0, 2, . . It is evident that ℓ_0 and ℓ'_0 must have opposite parities with each other because $\ell_0 + \ell'_0 + k =$ even. One can put $\phi_k = \phi_K = 0$ in the arguments of the spherical harmonics $Y_{k,\mathcal{M}-\mathcal{M}'}$ and $Y_{L_0,M-M'}$, because there is no $\phi_k = \phi_K$ dependence because of the relation of $\mathcal{M} - \mathcal{M}' = -(M - M')$.

[1] H. Outa *et al*., Nucl. Phys. **A754**, 157c (2005).
[2] B. H. Kang *et al*., Phys. Rev. Lett. **96**, 062301 (2006).
[3] M. J. Kim *et al*., Phys. Lett. **B641**, 28 (2006).
[4] T. Maruta *et al*., Nucl. Phys. **A754**, 168c (2005).
[5] T. Maruta, Ph. D. thesis, KEK Report 2006-1, 2006.
[6] S. Ajimura *et al*., Phys. Rev. Lett. **84**, 4052 (2000).
[7] K. Itonaga, T. Ueda, and T. Motoba, Nucl. Phys. **A577**, 301c (1994); **A585**, 331c (1995); in *Proceedings of the IV International Symposium on Weak and Electromagnetic Interactions in Nuclei*, edited by H. Ejiri, T. Kishimoto, and T. Sato (World Scientific, Singapore, 1995), p. 546.
[8] K. Itonaga, T. Ueda, and T. Motoba, Phys. Rev. C **65**, 034617 (2002).
[9] K. Itonaga, T. Motoba, and T. Ueda, in *Proceedings of the International Symposium on Electrophotoproduction of Strangeness on Nucleons and Nuclei*, edited by K. Maeda, H. Tamura, S. N. Nakamura, and O. Hashimoto (World Scientific, Singapore, 2004), p. 397.
[10] A. Parreño, A. Ramos, and C. Bennhold, Phys. Rev. C **56**, 339 (1997).
[11] D. Jido, E. Oset, and J. E. Palomar, Nucl. Phys. **A694**, 525 (2001).
[12] A. Parreño and A. Ramos, Phys. Rev. C **65**, 015204 (2002).
[13] G. Garbarino, A. Parreño, and A. Ramos, Phys. Rev. C **69**, 054603 (2004).
[14] K. Sasaki, T. Inoue, and M. Oka, Nucl. Phys. **A669**, 331 (2000); **A678**, 455(E) (2000).
[15] K. Sasaki, T. Inoue, and M. Oka, Nucl. Phys. **A707**, 477 (2002).
[16] Assumpta Parreño, Cornelius Bennhold, and Barry R. Holstein, Phys. Rev. C **70**, 051601 (2004); Nucl. Phys. **A754**, 127c (2005).
[17] J.-H. Jun, Phys. Rev. C **63**, 044012 (2001).
[18] A. Ramos, E. van Meijgaard, C. Bennhold, and B. K. Jennings, Nucl. Phys. **A544**, 703 (1992).
[19] W. M. Alberico, G. Garbarino, A. Parreño, and A. Ramos, Phys. Rev. Lett. **94**, 082501 (2005).
[20] C. Barbero, A. P. Galeão, and F. Krmpotić, Phys. Rev. C **72**, 035210 (2005).
[21] K. Sasaki, M. Izaki, and M. Oka, Phys. Rev. C **71**, 035502 (2005).
[22] C. Chumillas, G. Garbarino, A. Parreño, and A. Ramos, Phys. Lett. **B657**, 180 (2007).
[23] C. Barbero and A. Mariano, Phys. Rev. C **73**, 024309 (2006).
[24] Th. A. Rijken, Phys. Rev. C **73**, 044007 (2006).
[25] Th. A. Rijken and Y. Yamamoto, Phys. Rev. C **73**, 044008 (2006); Th. A. Rijken and Y. Yamamoto, nucl-th/0608074.
[26] H. Ejiri, T. Kishimoto, and H. Noumi, Phys. Lett. **B225**, 35 (1989).
[27] K. Itonaga, T. Motoba, O. Richter, and M. Sotona, Phys. Rev. C **49**, 1045 (1994); K. Itonaga, T. Motoba, and M. Sotona, Prog. Theor. Phys. **117**, 17 (1994).
[28] M. M. Block and R. H. Dalitz, Phys. Rev. Lett. **11**, 96 (1963).
[29] S. Ajimura *et al*., Phys. Lett. **B282**, 293 (1992).
[30] Particle Data Group, J. Phys. G **33**, 1 (2006).
[31] K. Itonaga *et al*. (in preparation).
[32] J. Schwinger, *Particles and Sources* (Gordon and Breach, New York, 1969).
[33] A. Ramos, E. Oset, and L. L. Salcedo, Phys. Rev. C **50**, 2314 (1994).
[34] Y. Sato *et al*., Phys. Rev. C **71**, 025203 (2005).
[35] M. M. Nagels, T. A. Rijken, and J. J. de Swart, Phys. Rev. D **12**, 744 (1975); **15**, 2547 (1977).